Phase diagram and snap-off transition for twisted party balloons

Yu-Chuan Cheng,[1] Ting-Heng Hsieh,[1] Jih-Chiang Tsai,[2] and Tzay-Ming Hong[1,*]
[1]*Department of Physics, National Tsing Hua University, Hsinchu, Taiwan 30013, Republic of China*
[2]*Institute of Physics, Academia Sinica, Taipei, Taiwan 11529, Republic of China*

(Received 24 December 2020; revised 23 June 2021; accepted 28 September 2021; published 19 October 2021)

Many of us have the experience of inflating balloons and twisting them into different shapes and animals. Snapping the balloon into two separate compartments is a necessary step that bears resemblance to the pinch-off phenomenon when a water droplet detaches from the faucet. In addition to testing whether balloons exhibit the properties of self-similarity and memory effect that are often associated with the latter event, we determine their phase diagram by experiments. It turns out that a common party balloon does not just snap, but can assume five more shapes, i.e., straight, necking, wrinkled, helix, and supercoil, depending on the twist angle and ratio of its length and diameter. Moreover, history also matters due to their prominent hysteresis. One may shift the phase boundary and/or reshuffle the phases by untwisting or lengthening the balloon at different twist angle and initial length. A heuristic minimal model is provided to obtain analytic expressions for the phase boundaries.

DOI: 10.1103/PhysRevE.104.045004

I. INTRODUCTION

Twisting and bending elastic filaments [1–3] or ribbons [4,5] has fascinated scientists for centuries, such as a coil formed by twisting a rope [6] and tendril of the climbing plant [7,8]. In recent years, due to the progress in biology, researches in DNA and protein structures and functions make this topic popular again [9–11]. For a long rod or wire, a one-dimensional description suffices since the thickness is much smaller than the length. In this work, we shall investigate the twisting of inflated party balloons in Fig. 1(a) for which the rubber thickness t is replaced by radius R that is comparable to length L.

Balloon is an example of soft material that is easily accessible and fun to play with. When inflated with air or fluid, it exhibits many interesting phenomena, such as a longitudinal phase separation during inflating [12–16], deformation and bursting when it impacts a rigid wall [17], fragmentation due to bursting [18], and air transfer between two balloons [19]. Our initial goal is to determine how many configurations a twisted balloon can adopt besides the familiar snapping phase. It turns out that the phase diagram is not a state function of the twist angle θ and ratio of length and diameter, but also depends on history, e.g., untwist or increase $L/2R$ while fixing the θ. This hysteretic behavior is more extensive than that for a stretched loop ribbon [5], the rearrangements of soap films in a triangular prism frame [20], and when the frequency of an applied force to zip or unzip DNA is varied [21]. It is hard not to see some resemblance between the snap-off transition and the pinch-off phenomenon for water dripping from a faucet [22,23], bubble formation [24,25], elephant trunks of interstellar gas and dust in the Eagle Nebula [26], and the sticky "capture blob" used by Bolas spider [26]. Comparisons are made in the end.

II. EXPERIMENTAL SETUP

Produced by Sempertex, our balloon samples come in three diameters, 1, 2, and 3 inches when inflated. They can be blown up to 60 inches long—about five times their original length. When inflated, their material characteristics are: Young's modulus $Y = 0.02$ GPa, thickness $t = 0.07$ mm, and shear modulus $S = 1$ MPa.

The experimental setup in Fig. 1(b) consists mainly of two parts, a frictionless rail and a force sensor. The rail is composed of two hollow coaxial cylinders, A and B, through which the balloon is inserted. Cylinder A is the active side via which we twist the balloon around a bearing fixed on a desk. As the stepping motor rotates at a steady angular velocity, a tension meter measures the twist force F.

In Fig. 1(b), the inner diameter of A and B is adjustable. While being prevented from rotating about A by a weight of 600 gw, the cylinder B is fixated to a long hollow aluminum pipe of length $S_E = 1$ m that is much larger than its diameter $s = 1$ cm. A long iron centering pin fixed to the ground is then inserted into the pipe to avoid tilting that may otherwise happen when the balloon tries to bend to lessen its shear energy which renders the twist angle hard to control. In the mean time, the combination of wires of length $W = 5$m and sliding rails that are fixed on the ceiling ensures that the cylinder B moves passively along the central axis as long as the displacement $\Delta z \ll W\sin\alpha$ where α denotes the angle between the wire and ceiling in Fig. 1(b).

III. A CONSERVED PHYSICAL QUANTITY

Let us first examine a straight twisted balloon. The shear modulus S is defined as the ratio of shear stress $F/(2\pi Rt)$ to

*ming@phys.nthu.edu.tw

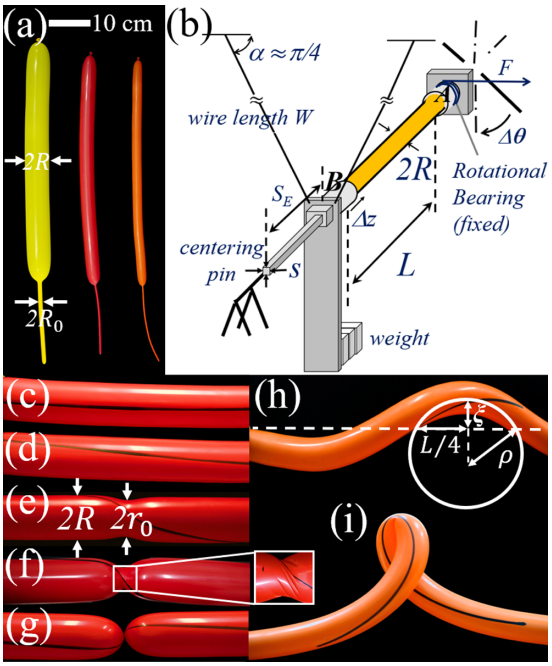

FIG. 1. (a) Balloon samples. (b) An inflated balloon is inserted and fastened by Velcro straps between two cylinders where A is driven by a stepper motor and in charge of twisting. The operational length L is defined as the distance between the inside edge of Velcros. (c) A horizontal mark is drawn before twist. Besides the straight phase in panel (d), a medium-sized balloon with $L/2R = 4.6$ can develop (e) necking, (f) wrinkles, and (g) snapping. In contrast, a long balloon with $L/2R = 11.8$ shows (h) helix and (i) supercoil. The white circle in panel (h) is to facilitate visualization of the relation between the two radii of curvature, ρ and ξ.

the shear strain ϕ where $2\pi Rt$ is the cross section area:

$$S = \frac{\frac{F}{2\pi Rt}}{\phi}. \tag{1}$$

When we twist the balloon by angle θ, as shown in Fig. 2(a), the arc length $\overset{\frown}{CD} = R\theta$. From the perspective of L, $\overset{\frown}{CD}$ is achieved by twisting angle ϕ. Therefore,

$$R\theta = L\phi, \tag{2}$$

as long as $\phi \ll 1$ which is obeyed in the parameter range we tested. Combining Eqs. (1) and (2), we obtain

$$F = S \times 2\pi Rt\phi = S\frac{2\pi R^2 t}{L}\theta. \tag{3}$$

As will be explained soon, a part of the balloon may become concave at large enough θ. Ostensibly it seems energetically unfavorable for the balloon to voluntarily concave because it raises the surface tension energy. So the balloon must have been compensated by the shear energy. To see why, let us generalize Eq. (1) to a balloon with a nonuniform transverse radius $r(z)$. The elasticity relation for shearing becomes

$$\frac{F}{2\pi rt} = S\frac{r\,d\theta(z)}{\sqrt{(dz)^2 + (dr)^2}}, \tag{4}$$

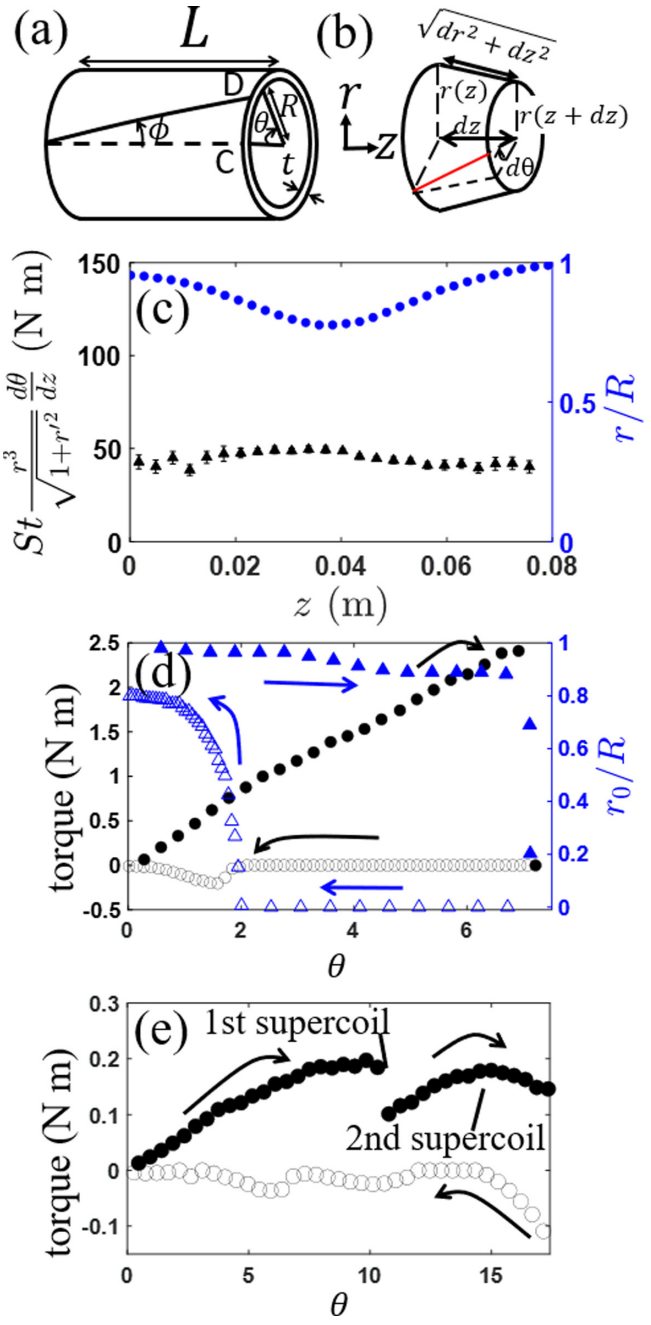

FIG. 2. (a) A schematic of a twisted balloon in phase 1. (b) A thin slice of vertical cross section between z and $z + dz$. (c) The conserved quantity in Eq. (5) is checked and shown by triangles for a concave balloon with $L/2R = 2.0$ and $\theta = 4.0$ whose profile is denoted by circles in the second y axis on the right. The r-dependence of St and how to measure r are elaborated in Sec. III of the Supplemental Material (SM) [27]. Circle and triangle in (d) represent torque and minimum radius r_0, with solid and open symbols denoting twist and untwist, in the double-y plot vs θ for $L/2R = 5.0$. (e) is for $L/2R = 14$. Note that r_0 does not pop back to full R as θ is relaxed to 0 in (d).

for the slice between z and $z + dz$ in Fig. 2(b) where $\theta(z)$ is the local twist angle that obeys $\theta(L) =$ total twist angle θ, $dr \equiv r(z + dz) - r(z)$ denotes the difference between local radius, and dr and dz are the two sides of rectangle whose hypotenuse

$\sqrt{(dz)^2+(dr)^2}$ plays the role of L in Eq. (3). By combining Eq. (4) with the constant torque condition, $Fr = \text{const.}$, from static equilibrium, we obtain

$$St\frac{r^3}{\sqrt{1+(dr/dz)^2}}\frac{d\theta(z)}{dz} = \text{const.} \tag{5}$$

This conserved quantity is verified in Fig. 2(c) for the concave and smooth region where S and t are respectively an decreasing and increasing function of r but their product St is found to be roughly a constant by Fig. S4(g) of the SM [27]. The r^3 in Eq. (5) implies that lowering r can redirect more shear angle into the concave segment and lower the total shear energy, as demonstrated in Sec. VII of the SM [27].

IV. MECHANICAL RESPONSE AND HYSTERESIS

In the following, we refer medium balloons to $4 < L/2R \leqslant 8$. As shown in Figs. 1(c)–1(g), their configuration evolves continuously from being (1) straight and smooth to (2) concave and smooth and (3) concave and wrinkled. At the point of (4) snapping in Fig. 1(g), the balloon suddenly loses its resistance. The transition in Fig. 2(d) is abrupt. Live demonstrations can be found in Video S1 in the SM [27].

For a long balloon in Fig. 2(e), phases (2∼4) are now replaced by (5) helix and (6) supercoil, as shown in Figs. 1(h) and 1(i). The torque plummets at the border between phases 5 and 6. There is no such a discontinuity for later transitions when more supercoils take turns to appear. By examining the marker line on the balloon and other reasons detailed in Sec. IV and Video S1 of the SM [27], we know that shear stress hardly affects the bended region, i.e., the supercoil. Phases 5 and 6 are shared by twisted filaments [6] whose torque versus θ relation is similar to Fig. 2(e).

Hysteresis is observed when the balloon is allowed to untwist. The torque in Fig. 2(d) changes continuously to the best resolution of our force meter from phase 4 to 3, and the neck radius does not pop up to full R until θ is much smaller than the critical angle when phase 1 transits to 2 in the forward twist process. This relaxation line is reversible until it meets the forward twisting line that will take over the evolution. We believe hysteresis is intrinsic and not due to plasticity that is present in balloons since r_0 did not revert to R at $\theta = 0$ in Fig. 2(d). Our proof comes from testing on an inflated condom [27] that is mainly plastic, but still exhibits the hysteresis.

V. MINIMAL MODEL FOR PHASE BOUNDARIES

Shear energy for phase 1 can be written down as

$$E_1 \sim SRtL\left(\frac{R\theta}{L}\right)^2 = \frac{SR^3t}{L}\theta^2. \tag{6}$$

For phase 2, we approximate the concave segment by a uniform tube of length ℓ, radius $r \leqslant R$, and shear angle θ_1 to obtain

$$E_2 \sim \frac{Sr^3t}{\ell}\theta_1^2 + \frac{SR^3t}{(L'-\ell)}(\theta-\theta_1)^2 + 2\pi T[R(L'-\ell)+r\ell+(R^2-r^2)-RL], \tag{7}$$

where T denotes the surface tension coefficient, defined as the amount of stretching energy per unit surface area and the empirical value is about 55.5J/m^{-2} in inflated state. The first two terms represent the separate contributions from the concave region and the rest of surface. Since we treat the air as being incompressible, the air that originally occupies the concave region will be relocated and elongate the balloon from its original length L to L'. By volume conservation, we obtain the following:

$$\pi R^2 L = \pi R^2(L'-\ell) + \pi r^2\ell, \tag{8}$$

where $L'-\ell = L-(r^2/R^2)\ell$. By use of Eq. (8), the conserved quantity in Eq. (5) requires that

$$\frac{r^3\theta_1}{\ell} = \frac{R^3(\theta-\theta_1)}{L-\frac{r^2}{R^2}\ell}, \tag{9}$$

which pins down θ_1 as a function of r and ℓ which in turn are determined by minimizing E_2 respectively, as detailed in Sec. VII of the SM [27]. Setting $r = R$ and equating Eqs. (6) and (7) reveal that

$$\ell \sim R \tag{10}$$

at the transition from phase 1 to 2 when the twist angle reaches

$$R\theta_{1,2}/L \sim \sqrt{T/(St)}, \tag{11}$$

which matches the data in Fig. 3(a). Let us skip E_3 since its transition from phase 2 is empirically difficult to nail down. The next is phase 4. By now, the marker line on balloon has reverted to being horizontal at the snap-off and, therefore, we do not expect any remaining shear energy except the creation of two hemispheres about the singular neck. So,

$$E_4 \sim TR^2. \tag{12}$$

Physically we expect the snap-off to be triggered by an imbalance between shear and surface energies. In other words, the transition angle $\theta_{3,4}$ can be estimated by equating Eqs. (6) and (12):

$$\theta_{3,4} \sim \sqrt{\frac{T}{St}\frac{L}{R}}. \tag{13}$$

The reason why we did not try to incorporate the wrinkles and write down E_3 is that the snap-off transition is abrupt so that $E_3 > E_4$ and $\theta_{3,4}$ cannot be determined by equating them.

Phase 5 for long balloons is trickier in that it relieves part of the shear energy by angle η by distorting or bending itself into a helix. Furthermore, a second bending term is needed because our experimental setup in Fig. 1(b) requires both ends of the balloon aligned. By twiddling with real balloons, it is easy to realize that this extra energy (1) is redundant for $\eta = 0$ and 2π when the alignment is automatic, and (2) can be diminished by lengthening the balloon which justifies an additional factor of R/L. Overall, we expect

$$E_5 \sim \frac{SR^3t}{L}(\theta-\eta)^2 + K_b\left(\frac{\eta}{L}\right)^2 RL + K_b\frac{\eta(2\pi-\eta)}{L^2}R^2, \tag{14}$$

where $K_b \sim YR^2t$ from elasticity and η/L in the second term coming from the curvature $1/\rho$ that can be derived from the

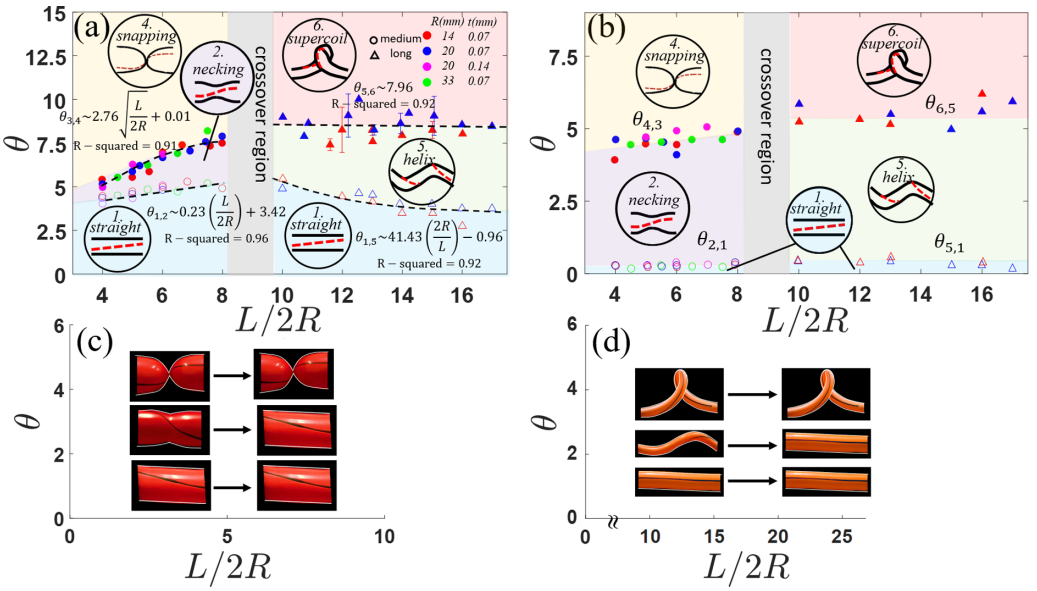

FIG. 3. Phase diagram for balloons is history-dependent. Panel (a) is for a twisted balloon with fixed $L/2R$ where doubling t is achieved by inserting one balloon into another before inflating which also doubles T in Eq. (11). Open symbols denote the transition angle $\theta_{1,2}$ and $\theta_{1,5}$, and solid symbols are for $\theta_{3,4}$ and $\theta_{5,6}$. Dashed lines are the fitting functions. Gray area means there exists a crossover region for the transition. Panel (b) is obtained by untwisting a snap-off or supercoil balloon. Note that $\theta_{2,1}$ refers to the transition angle from phase 2 to 1, and same for others. Diagram (c) is by lengthening L while fixing R and θ for a short or medium balloon. Similar to panel (c), panel (d) is for a long balloon. Phase 3 is omitted since its range is too small.

Pythagorean theorem in Fig. 1(h), $\rho^2 = (\rho - \xi)^2 + (L/4)^2$, that requires $\rho \sim L^2/\xi$. The fact that ξ is linked to η by $\xi \sim \eta L$ immediately leads to $\rho \sim L/\eta$.

Minimizing Eq. (14) with respect to η gives

$$\eta \sim \frac{S\theta - Y\frac{R}{L}}{S + Y(1 - \frac{R}{L})}. \tag{15}$$

For phase 1 to enter phase 5 and η to increase from zero, Eq. (15) sets a lower bound on θ that can be duly identified as the boundary

$$\theta_{1,5} \sim \frac{Y}{S}\frac{R}{L}. \tag{16}$$

As the twisting continues, we come to the next boundary by setting $\eta = 2\pi$ in Eq. (14). This renders

$$\theta_{5,6} \sim 2\pi + \frac{Y}{S}, \tag{17}$$

independent of L, R. The same conclusion has been derived [34] for a twisted filament, which implies that the much larger length scale L in the longitudinal direction masks the structure in the cross section. This is similar to the fact that the lattice spacing becomes negligible when taking the long-wavelength limit for the dispersion relation of phonons in solid.

Vindicated by the R-squared values shown in Fig. 3(a), the theoretically predicted dependence of phase boundaries on $L/2R$ matches the experiment excellently. In addition, the prefactors also fall in the right ballpark. For instance, $\sqrt{T/(St)}$ in Eqs. (11) and (13) equals 0.890 in contrast to the empirical value of 0.23 and 2.76. As for Eqs. (16) and (17), the factor of Y/S equals 20.30 as opposed to 41.43 and 7.96 from the fitting. The discrepancy is expected since we have not been careful with numerical factors like $1/2$ and 2π to focus on the key experimental parameters in our minimal model. It is not worthwhile to go back and fill in these numbers since a bigger uncertainty lies in our approximating the concave region of a phase-2 balloon in Fig. 1(e) by a U-shape basin in Fig. S9(b). We have tried V-shape and smooth functions such as the Cauchy and Gaussian distributions, but the calculations quickly became so cumbersome that analytic expressions were no longer possible.

A closer scrutiny of the fitting functions in Fig. 3(a) will reveal the existence of constant terms not predicted by our model. They are an artifact of how we implemented the torque. Similar to how we grasp and twist the balloon by bare hands, we inserted the balloon into two hollow coaxial cylinders before fastening it by Velcro straps. As marked in Fig. 1(b), the operational definition of L is the distance between the inside edge of these two straps. Although we have tried to extend the reach of Velcros as far as possible, the ends of balloon, i.e., two hemispheres, inevitably stuck out and were not counted in the theoretical definition of L in Eq. (8) for a whole balloon whose volume is conserved. Therefore, when examining the empirical phase diagram of Fig. 3(a), all the theoretical L in this section need to be adjusted to $L + \Delta L$ where $\Delta L \approx 4.3R$ denotes the total length of two Velcro width and two radii of hemisphere. This change will introduce a positive correction to $\theta_{1,2}$ and $\theta_{3,4}$ since their L-dependence is in the numerator, as opposed to a negative amendment from the L in the denominator of $\theta_{1,5}$. More statistical analyses on the selection of a better fitting function can be found in Sec. IX of the SM [27].

Having established in Figs. 2(d) and 2(e) that the value of torque and r_0 for untwist is different from that for twist at the same θ, we thus expect a different phase diagram for relaxation. As plotted in Fig. 3(b), it becomes clear that the

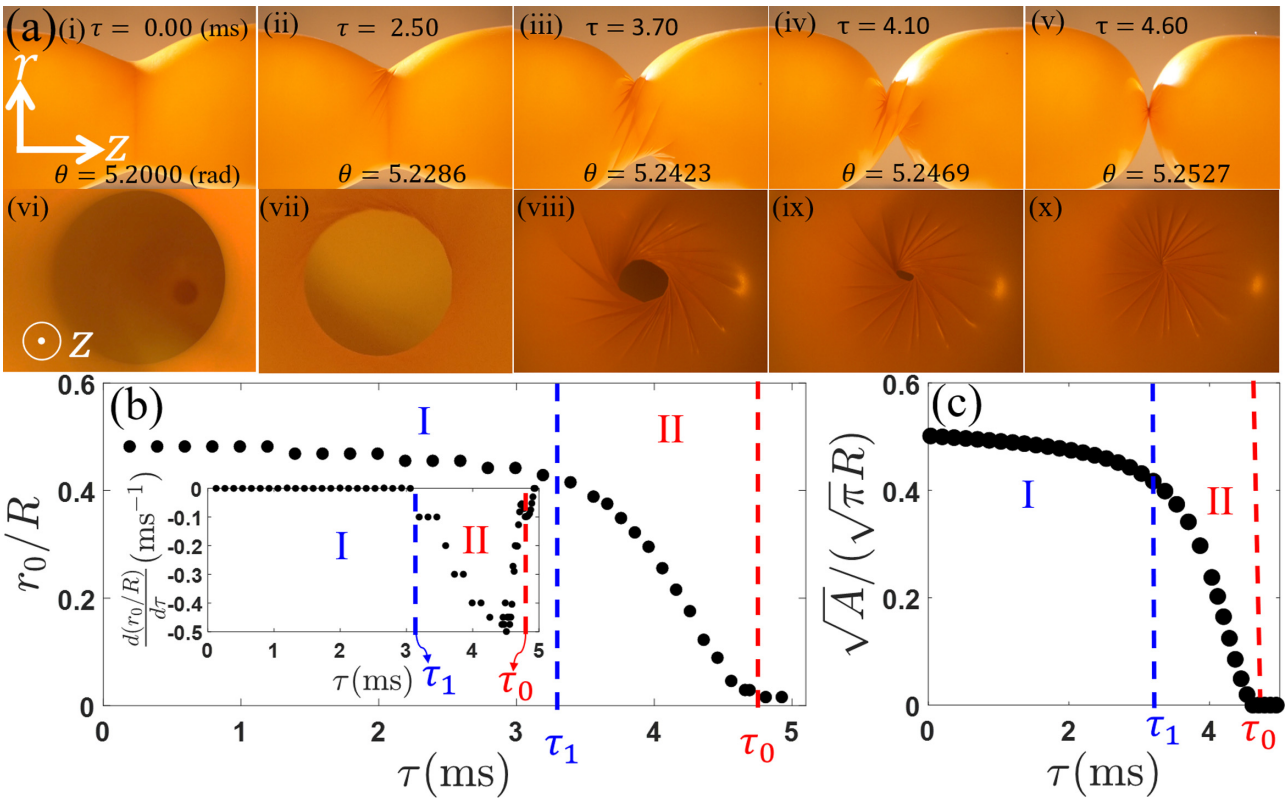

FIG. 4. (a) The evolution of configuration for a balloon with $L/2R = 4.6$ is shown by the side view in photographs (i–v). The closure of open area A at the bottleneck from the internal view in (vi–x), shot at the same time as the photograph above it. As can be viewed from Video S2 in the SM [27], both r_0 and A decrease slowly at the final moment of snap-off, which made them unsuitable to define τ_0. (b) Dimensionless radius r_0/R vs real time τ. The first derivative is plotted in the inset where the vertical dash lines mark the time τ_0 and τ_1 at which the speed equals 10% of its maximum value. We set $\tau < \tau_1$ as regime I when the neck radius hardly decreases, as opposed to regime II for $\tau_1 < \tau < \tau_0$ when the irreversible and automatic shrinkage picks up a noticeable speed. The temporal resolution is 0.1 ms. (c) Equivalent radius of the open hole in (vi-x) vs τ where $\tau_0 = 4.60$ ms corresponds to the full closure of the shutter.

phase boundaries, $\theta_{4,3}$ and $\theta_{2,1}$ are indeed dissimilar to $\theta_{3,4}$ and $\theta_{1,2}$. For instance, $\theta_{2,1} \sim \theta_{5,1} \sim 0.1$ is small for all lengths, in contrast to Eqs. (11) and (16). The story does not end here that two more different phase diagrams are found when we lengthen L while keeping θ fixed. Experimentally this is achieved by shifting the moving end B in Fig. 1(b) while holding the balloon (to keep the twist angle fixed.) If we start from phase 4, then it remains so without entering phase 6, as shown in Fig. 3(c). But if we start from phase 5, it will transit to phase 1 in Fig. 3(d).

VI. DETERMINATION OF SNAP-OFF TIME AND SHRINKING SPEED

A high-speed camera with 10 000 fps was used to capture the dynamical process that leads up to a singular neck. The balloon in Figs. 4(a)(i), 4(a)(ii), and 4(a)(iii) is reversible and corresponds to phases 2 and 3, respectively. Being taken at successive time at the same θ, the process in Fig. 4(a)(iv) and 4(a)(v), categorized as phase 4, thus reveals their irreversibility. Note that the exact time τ_0 at which the snap-off occurs is not as clear-cut as its counterpart for pinch-off because the two disconnected segments of balloon remain attached and r_0 never equals exactly zero in Fig. 4(a). Additionally, r_0 approaches zero at only 1% of the maximum speed which makes it difficult to single out a value that corresponds to τ_0. So we resort to its time-derivable for a clearer identification. Analogous to the cutoff frequency in filters [35], τ_0 and another threshold time τ_1 can be unambiguously defined through the caption for the inset of Fig. 4(b) to signalize regime II during which period the shrinking and its accompanying physics mainly occur. It comes as no surprise that τ_0 roughly coincides with the time when the opening in Fig. 4(c) vanishes because further shrinkage beyond this point will squeeze on the rubber. Evidence presented in Sec. X of the SM [27] indicates that, while τ_0 is an important parameter for characterizing the properties for snap-off transition, there is a tolerance range of 0.5 ms to its precise value.

Unlike the reversible regime I where dr_0/dt is determined by the stepper motor, an average shrinking speed v_s for regime II in Fig. 5(a) is meaningful because it is intrinsic to the phase-4 balloon. In Figs. 5(b) and 5(c), $\tau_0 - \tau$ is rendered dimensionless by an intrinsic timescale that comes from dividing R by a characteristic speed v whose expression will be theoretically derived shortly in Eq. (22). As proven in Sec. X of the SM [27] by the calculation of cosine similarity value [36] that exceeds 0.9, we are confident to claim that medium balloons exhibit the property of self-similarity in regime II,

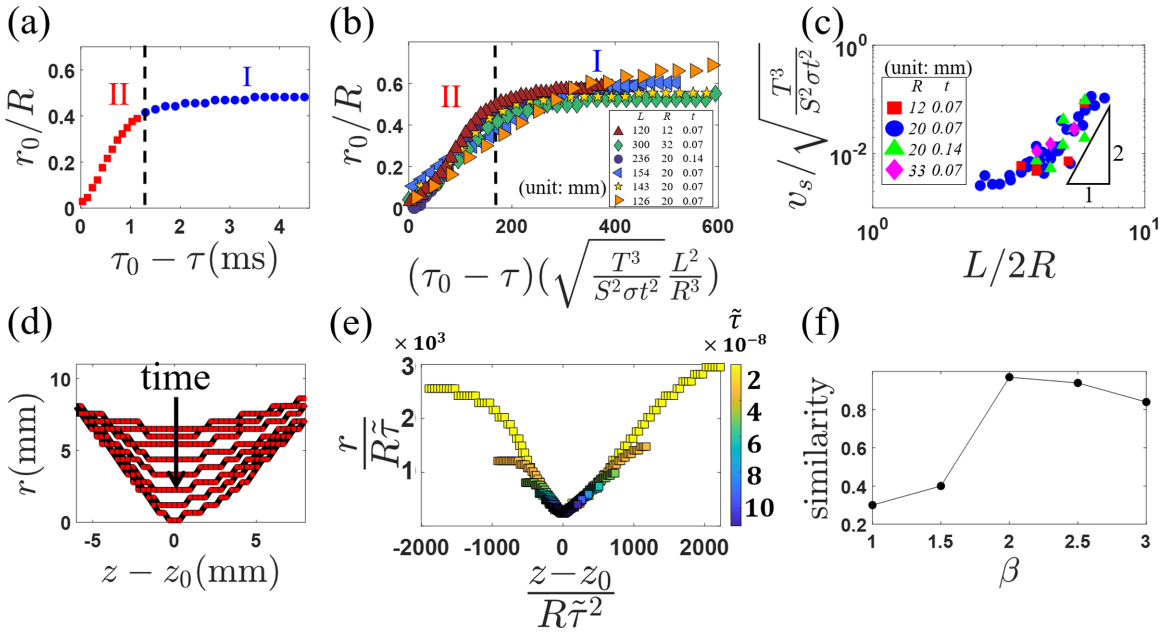

FIG. 5. (a) Figure 4(b) is replotted by shifting τ to $\tau_0 - \tau$. Dash line at $\tau = \tau_1$ signalizes the transition from reversible to irreversible. (b) By renormalizing the x axis in panel (a), data for different L, R, and t can be made to collapse to a master curve in regime II. (c) Renormalized shrinking speed v_s increases quadratically with $L/2R$. (d) Time evolution of balloon profile where z_0 is the position at the bottleneck. The time interval between successive lines is 0.1 ms. (e) Data in regime II can be made to collapse to a master curve by rescaling. (f) Cosine similarity value is evaluated for different β.

i.e., the data for different R, L, and t can be made to collapse onto one master curve by rescaling. A direct vindication for v can be found in Fig. 5(c) where the empirically obtained v_s is shown to scale with v. To test whether snap-off transition exhibits the property of self-similarity, we rescale the profiles in Fig. 5(d) by $r/(R\tilde{\tau}^{\alpha})$ and $(z - z_0)/(R\tilde{\tau}^{\beta})$ where $\alpha = 1$ and $\beta = 2$ enable the best overlap in Fig. 5(e) via trial and error. Physically, the scaling exponent $\alpha = 1$ is expected from the constant v, but $\beta = 2$ is determined by maximizing the cosine similarity value in Fig. 5(f). Note that the relative magnitude of $\alpha < \beta$ is different from $0 < \beta \leqslant \alpha \leqslant 1$ for pinch-off systems [23]. For starters, rubber does not obey the Rayleigh-Plateau instability that predicts the breakage of water column occurs when $r \leqslant z - z_0$. Therefore, $\beta - \alpha < 0$ is required to revert the relative size in

$$\frac{r}{\tilde{\tau}^{\alpha}} > \frac{z - z_0}{\tilde{\tau}^{\beta}} \tilde{\tau}^{\beta-\alpha} \tag{18}$$

at small $\tilde{\tau}$.

In the following, we explain that the quadratic relation between v and $L/2R$ comes from ratio of area between flat and neck regions, $A_{\text{flat}}/A_{\text{neck}}$, because longer balloons convert more shear potential into the kinetic energy of the collapsing neck. Since r is much smaller than R at the snap-off transition, $r^2\ell/R^2$ term can be neglected compared to L in both the numerator and denominator of Eq. (9). Furthermore, the first term r^3L in the denominator can be omitted because $R^3\ell$ is much larger. Based on the above approximations, Eq. (9) can be simplified to

$$\theta - \theta_1 = \frac{r^3 L}{R^3 \ell} \theta_1. \tag{19}$$

Remember that the distinction between short and medium balloons lies in whether the concave segment spans over the whole balloon. This is based on the result in Eq. (10), namely, $\ell \approx R$ at $\theta_{1,2}$. Now imagine cranking up θ in phase 2. Experimentally both r and ℓ are deceased instead of creating another partial segment with aggravated concaveness. This implies that the concave segment can be effectively treated as a downsized short balloon, and $r \sim \ell$ should be valid throughout phases 2 and 3. As a result, we can set $r \sim \ell = \delta R$ at the snap-off transition where $\delta \ll 1$ decreases with increasing θ. Apparently the twisting direction is arbitrary and so δ ought to be an even function of θ and $\delta \sim 1/\theta^2$ is the simplest guess:

$$r \sim \ell \sim \frac{R}{(\theta_{3,4})^2} = \frac{SR^2 t}{TL} \tag{20}$$

at the snapping where the expression for $\theta_{3,4}$ has been borrowed from Eq. (13). Finally, the shear strain accumulated outside of the concave segment is "sucked" into the bottleneck because $d\theta/dz$ diverges at $r \to 0$ according to Eq. (5). This shear energy is then converted to the kinetic energy of shrinking:

$$\frac{SR^3 t}{L}(\theta - \theta_1)^2 \sim \frac{\sigma}{2} \ell r v^2 = \frac{\sigma}{2} \left(\frac{SR^2 t}{TL} \right)^2 v^2, \tag{21}$$

where σ is the surface mass density and Eq. (20) has been used. Inputting the formula for $\theta - \theta_1$ in Eq. (9) then enables us to determine the shrinking speed as

$$v \sim \left(\frac{L}{R} \right)^2 \sqrt{\frac{T^3}{S^2 \sigma t^2}}. \tag{22}$$

TABLE I. Competing mechanisms in pinch-off and snap-off.

Phenomena		Pinch-off [23]	Snap-off
Singularity		Yes	Yes
Competing mechanisms	Input	Surface tension	Shear (dominant)
	Output	Viscosity (dominant)	Surface tension Inertia
		Inertia	

It is worth noting that this dependence on the initial length violates the lack of memory effect which property is often flaunted for pinch-off systems where v only depends on the flow of inner liquid [37,38].

VII. COMPARING SNAP-OFF TRANSITION WITH PINCH-OFF PHENOMENA IN FLUID

In spite of the analogy to the similarly abrupt and singular nature of pinch-off phenomenon [23,39–47], we emphasize that they do not share the same microscopic mechanisms. Shear trumps the surface tension as the main input energy to trigger the snap-off in balloons, and competes with dissipations due to the inertia of collapsing neck, as summarized in Table I. A clear physical insight is via the inspection of the conserved quantity derived in Eq. (5) and vindicated by Fig. 2(c), which states that $d\theta/dz$ is proportional to r^{-3}. This sensitive dependence predicts that the shear strain, along with its energy, will be pumped *en masse* in the immediate vicinity of the singular neck as $r \to 0$. This picture is backed up by the experimental observation that the marker line on the flat segments that flank the concaved region suddenly reverts to being horizontal upon the occurrence of snap-off. This is clear evidence that shear energy is being converted to the kinetic energy of the collapsing neck. Unlike the Rayleigh-Plateau instability, the surface tension energy plays a lesser role in balloons. This can be easily demonstrated by pinching the neck of an untwisted balloon, which will not create the abruptness characteristic of the snap-off transition.

VIII. CONCLUSION AND DISCUSSIONS

In summary, we show that party balloons can assume six configurations, depending on the twist angle and aspect ratio between length and diameter. Scaling analysis, including the finding of a conserved quantity that links radius and the gradient of strain, are provided to derive analytical forms for the phase boundaries that are consistent with experimental findings. Not caused by the plasticity, the hysteresis of balloon is pronounced that the allowed number of phases and their location in the phase diagram are subject to change when the balloon is untwisted or lengthened at different twist angle and initial length.

Special attention is paid to clarify the connection between the snap-off and pinch-off transitions. Although the finite thickness of rubber will prevent the balloon neck from actually collapsing to a singularity, the physics we are interested in happens prior to that. So the development of a neck whose size evolves to be much smaller than all the other length scales of the system is common in these two phenomena. Furthermore, they share the existence of two competing energies to safeguard the property of self-similarity. Mainly, the surface tension in pinch-off is replaced by shear in snap-off as the dominant input energy, while the dissipation from viscosity being negligible for air is substituted by the inertia term of the collapsing neck. It will be worthwhile to find and solve the counterpart of Stokes equation [23] for snap-off in the future to clarify the physical mechanism implied by the different scaling exponents.

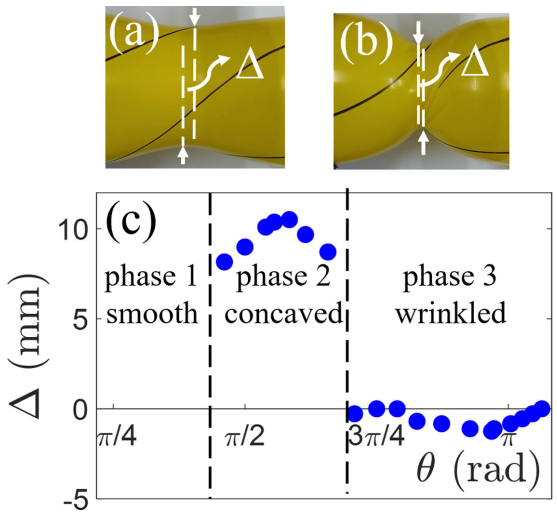

FIG. 6. (a, b) The asymmetry in phase 2 and 3 with $L/2R = 2$ and $\theta = 90^0$, 140^0 tilts in opposite directions. (c) The lateral shift Δ is plotted as a function of θ. The dash vertical lines denote the phase boundary.

While measuring the radius $r(z)$ for Fig. 2(c) to vindicate Eq. (5), we realized that the upper and lower profiles of phase-2 and -3 balloon are not symmetric. In other words, the twisted balloon automatically breaks its reflection symmetry in phase 2, but temporarily restores the symmetry at $\theta_{3,4}$ before breaking it again in phase 3 in a reversed direction, as demonstrated by Fig. 6. The lateral distance Δ denotes the shift between the lowest point of upper profile and the highest point of lower profile. We do not yet fully understand the mechanism that triggers this breaking of reflection symmetry, nor can we explain why the symmetry is restored temporarily at the critical angle. However, a useful clue is that Δ can be reversed if we change the chirality of the twisting direction. This strongly suggests that the act of twisting is responsible for breaking the symmetry.

ACKNOWLEDGMENTS

We thank Jow-Tsong Shy, Ching-Yao Lai, and Khá-Î Tô for fruitful discussions, and we gratefully acknowledge technical assistance from Yen-Ju Richard Huang, Chih-Tang Liao, Y.-L. Peng, Wei Chien, Chen-Man Tien, Hung-Chieh Fan Chiang, Wei-Chi Lee, and Hsin-Huei Li. We are also thankful to Pai-Yi Hsiao, Jung-Ren Huang, and Yeng-Long Chen for early discussions. This work was supported by MoST in Taiwan under Grants No. 105-2112-M007-008-MY3 and No. 108-2112-M007-011-MY3.

[1] A. Ghatak and A. Lal Das, Phys. Rev. Lett. **99**, 076101 (2007).
[2] H. Wada, Phys. Rev. E **84**, 042901 (2011).
[3] N. Charles, M. Gazzola, and L. Mahadevan, Phys. Rev. Lett. **123**, 208003 (2019).
[4] J. Chopin and A. Kudrolli, Phys. Rev. Lett. **111**, 174302 (2013).
[5] Y. Morigaki, H. Wada, and Y. Tanaka, Phys. Rev. Lett. **117**, 198003 (2016).
[6] A. Ghatak and L. Mahadevan, Phys. Rev. Lett. **95**, 057801 (2005).
[7] S. J. Gerbode, J. R. Puzey, A. G. McCormick, and L. Mahadevan, Science **337**, 1087 (2012).
[8] A. Goriely and M. Tabor, Phys. Rev. Lett. **80**, 1564 (1998).
[9] A. Dittmore, S. Brahmachari, Y. Takagi, J. F. Marko, and K. C. Neuman, Phys. Rev. Lett. **119**, 147801 (2017).
[10] S. Niewieczerzal and J. I. Sulkowska, Phys. Rev. Lett. **123**, 138102 (2019).
[11] C. Bouchiat and M. Mezard, Phys. Rev. Lett. **80**, 1556 (1998).
[12] A. Giudici and J. S. Biggins, Phys. Rev. E **102**, 033007 (2020).
[13] A. Mallock, Proc. R. Soc. London **49**, 458 (1891).
[14] E. Chater and J. W. Hutchinson, J. Appl. Mech. **51**, 269 (1984).
[15] B. Audoly and J. W. Hutchinson, J. Mech. Phys. Solids **97**, 68 (2016).
[16] B. Audoly and J. W. Hutchinson, J. Mech. Phys. Solids **123**, 149 (2019).
[17] E. Jambon-Puillet, T. J. Jones, and P.-T. Brun, Nat. Phys. **16**, 585 (2020).
[18] S. Moulinet and M. Adda-Bedia, Phys. Rev. Lett. **115**, 184301 (2015).
[19] Y. Levin and F. L. da Silveira, Phys. Rev. E **69**, 051108 (2004).
[20] N. Vandewalle, M. Noirhomme, J. Schockmel, E. Mersch, G. Lumay, D. Terwagne, and S. Dorbolo, Phys. Rev. E **83**, 021403 (2011).
[21] S. Kumar and G. Mishra, Phys. Rev. Lett. **110**, 258102 (2013).
[22] P. Doshi and O. A. Basaran, Phys. Fluids **16**, 585 (2004).
[23] I. Cohen, M. P. Brenner, J. Eggers, and S. R. Nagel, Phys. Rev. Lett. **83**, 1147 (1999).
[24] J. Erlebacher, Phys. Rev. Lett. **106**, 225504 (2011).
[25] L. Salkin, A. Schmit, P. Panizza, and L. Courbin, Phys. Rev. Lett. **116**, 077801 (2016).
[26] Reflections on a Liquid Drop, uploaded by The University of Chicago, 20 April 2016, www.youtube.com/watch?v=MwG3eODlDMw.
[27] See Supplemental Material at http://link.aps.org/supplemental/10.1103/PhysRevE.104.045004 for live videos and detailed calculations, which include Refs. [28–33].
[28] J. Wang, J. Sha, and W. Sun, Phys. Teach. **57**, 650 (2019).
[29] S. T. Tsai, C. D. Chang, C. H. Chang, M. X. Tsai, N. J. Hsu, and T. M. Hong, Phys. Rev. E **92**, 062925 (2015).
[30] H. Akaike, in *Proceedings of the 2nd International Symposium on Information Theory*, edited by B. N. Petrov and F. Csaki (Armenia, USSR, 1971), pp. 267–281; IEEE Trans. Auto. Control **19**(6), 716 (1974); *A Celebration of Statistics*, edited by A. C. Atkinson and S. E. Fienberg (Springer, Berlin, 1985), pp. 1–24.
[31] A. A. Pahlavan, H. A. Stone, G. H. McKinley, and R. Juanes, Proc. Natl. Acad. Sci. USA **116**, 13780 (2019).
[32] W. C. Li, C. Y. Shih, T. L. Chang, and T. M. Hong (unpublished).
[33] A. S. Utada, A. Fernandez-Nieves, H. A. Stone, and D. A. Weitz, Phys. Rev. Lett. **99**, 094502 (2007).
[34] A. Goriely and M. Tabor, Nonlin. Dyn. **21**, 101 (2000).
[35] M. E. Van Valkenburg, *Network Analysis*, 3rd ed. (Prentice-Hall, Englewood Cliffs, 1974), pp. 383–384.
[36] https://en.wikipedia.org/wiki/Cosine_similarity.
[37] X. D. Shi, M. P. Brenner, and S. R. Nagel, Science **265**, 219 (1994).
[38] P. Doshi, I. Cohen, W. W. Zhang, M. Siegel, P. Howell, O. A. Basaran, and S. R. Nagel, Science **302**, 1185 (2003).
[39] H. Y. Lo, Y. Liu, S. Y. Mak, Z. Xu, Y. Chao, K. J. Li, H. C. Shum, and L. Xu, Phys. Rev. Lett. **123**, 134501 (2019).
[40] L. K. Aagesen, A. E. Johnson, J. L. Fife, P. W. Voorhees, M. J. Miksis, S. O. Poulsen, E. M. Lauridsen, F. Marone, and M. Stampanoni, Nat. Phys. **6**, 796 (2010).
[41] J. R. Lister and H. A. Stone, Phys. Fluids **10**, 2758 (1998).
[42] J. Eggers, Phys. Rev. Lett. **71**, 3458 (1993).
[43] W. W. Zhang and J. R. Lister, Phys. Rev. Lett. **83**, 1151 (1999).
[44] M. Rubio, A. Ponce-Torres, E. J. Vega, M. A. Herrada, and J. M. Montanero, Phys. Rev. Fluids **4**, 021602(R) (2019).
[45] D. J. Ruth, W. Mostert, S. Perrard, and L. Deike, Proc. Natl. Acad. Sci. USA **116**, 25412 (2019).
[46] J. C. Burton, J. E. Rutledge, and P. Taborek, Phys. Rev. Lett. **92**, 244505 (2004).
[47] J. C. Burton and P. Taborek, Phys. Rev. Lett. **98**, 224502 (2007).